Hyperspectral portable beam transmissometer for the ultraviolet-visible spectrum

Shai Sabbah[1], James M. Fraser[2], Emmanuel S. Boss[3], Itamar Blum[4], and Craig W. Hawryshyn[1]*

[1]Department of Biology, Queen's University, 116 Barrie St., Kingston, Ontario, K7L 3N6, Canada
[2]Department of Physics, Engineering Physics, & Astronomy, Queen's University, Kingston, Ontario, K7L 3N6, Canada
[3]School of Marine Sciences, University of Maine, 5741 Libby Hall, Orono, Maine, 04469, USA
[4]Hazit 33, Karmy-Yosef, 99797, Israel

Abstract

The spectral beam attenuation coefficient is an important optical property of natural water used to quantify light propagation and visibility in the aquatic media, and to study the concentration of the water constituents. Although beam attenuation in the ultraviolet spectral range may be particularly informative, to date, no transmissometer capable of measuring the beam attenuation in the ultraviolet is commercially available. The portable hyperspectral beam transmissometer developed in our lab is capable of measuring across a broad spectral range (300–750 nm) at 2 nm spectral resolution. The transmissometer exhibits a small acceptance angle (0.55 to 0.59° across the spectrum), a well collimated spectral light beam, and precision of ±0.012 m^{-1}. The attenuation of diverse water samples measured with our transmissometer was found to be significantly similar to that measured with a commercially available transmissometer. Moreover, the attenuation of filtered samples, measured with our transmissometer, was significantly similar to their absorption, measured with a bench-top spectrometer. Testing the transmissometer in the field, the transmission of water samples collected in Lake Malawi, Africa, was measured on site. The magnitude and spectral shape of attenuation were in general agreement with previous reports. All assessment stages confirm the performance, accuracy, and applicability of our transmissometer. The extended spectral range and high spectral resolution of our portable transmissometer make it an excellent tool for studying the characteristics and distribution of dissolved and particulate matter in aquatic media and exploring the constraints imposed on the visibility and visual communication of aquatic organisms known to have ultraviolet photosensitivity.

Most of the earth's surface is covered with water. Marine and freshwater ecosystems are responsible for more than half of the world's net primary production (Field et al. 1998), and they harbor a huge diversity of organisms. Light harvesting by phytoplankton as well as aquatic animals' orientation, forag-

ing, courting, and visual communication all depend on the optical properties of the water environment. The spectral beam attenuation coefficient, $c(\lambda)$ [m^{-1}], is an important optical property of natural water used both to quantify light propagation in the aquatic media and visibility, and to study the concentration of the material affecting light propagation. The beam attenuation coefficient is typically derived from measurements performed using a beam transmissometer, which measures the intensity loss of a collimated light beam along a light path in water due to absorption and scattering, according to Beer-Lambert law (Jerlov 1976).

Transmission measurements are commonly used to obtain information on dissolved matter in the aquatic media. Additionally, these measurements are used in estimating the mass or volume concentration of particles in natural waters (Spinrad and Zaneveld 1982; Baker and Lavelle 1984). The wavelength dependence of the beam attenuation coefficient can be highly informative. For example, the spectral shape of particulate attenuation is used to obtain information on the size dis-

tribution of suspended particles (Volz 1954; Van De Hulst 1957; Diehl and Haardt 1980; Boss et al. 2001) and the bulk particulate refractive index (Twardowski et al. 2001). Several transmissometers, including the commonly used WET Labs ac-9 (412–715 nm; 9 wavelengths) and ac-s (400–730 nm; 4-nm interval), have been built to provide this spectral information (Petzold and Austin 1968; Matlack 1974; Lundgren 1975; Barth et al. 1997; Van Zee 2008). Whereas bench-top spectrometers and the recently developed in situ ISUS spectrophotometer (Satlantic) may measure the absorption of natural water in the ultraviolet (UV) range, to the best of our knowledge, no commercial transmissometer is capable of measuring beam attenuation in the UV spectral range. Knowledge of the attenuation and absorption in the UV range is important for several reasons. The attenuation of colored dissolved organic matter (CDOM) and particulates is typically high in the UV range (Jerlov 1976), and therefore, may provide insight into their source and chemistry. Absorption of dissolved materials, of which scattering is negligible (Stramski and Wozniak 2005), can be measured with a transmissometer following water filtration with a 0.2-μm filter (the difference between attenuation and absorption has been found to be negligible in that case). CDOM absorption in the UV is particularly important. CDOM undergoes photobleaching in the UV spectral region (Zepp 2003; Vahatalo and Wetzel 2004) and strongly affects UV light penetration into the aquatic media (Vahatalo and Wetzel 2004). Thus, measuring CDOM absorption in the UV may facilitate the study of CDOM characteristics and dynamics. Moreover, the concentration of nutrients such as nitrate, bromide, and bisulfide, which play a significant biogeochemical role in aquatic environments, can be estimated from the absorption in the UV (Johnson and Coletti 2002). Finally, the visual systems of many marine and freshwater fish and other aquatic organisms are sensitive to UV light (Hawryshyn and Beauchamp 1985; Losey et al. 1999; Marshall et al. 2007). To understand the visual constraints imposed on the detection and recognition abilities of such organisms and the role of UV signals in interspecific and intraspecific communication, knowledge of the beam attenuation in the UV range would be beneficial (Lythgoe and Partridge 1991; Marshall et al. 2003; Sabbah and Shashar 2006). Here we describe a hyperspectral portable transmissometer with a 2-nm spectral resolution across the UV-visible spectral ranges (300–750 nm) with precision of ±0.012 m⁻¹.

Materials and procedures

Transmissometer system setup—The transmissometer system consisted of three main components: (i) light source (DH-2000-BAL, Ocean Optics); (ii) a receiver system made of fiber-coupled modular spectroscopic system incorporating two identical spectrometers (Jaz, Ocean Optics); and (iii) a custom-built transmissometer consisting of optical assemblies and a flow tube (Fig. 1). The light source integrated two lamps, Tungsten-Halogen and Deuterium, providing a high and spec-
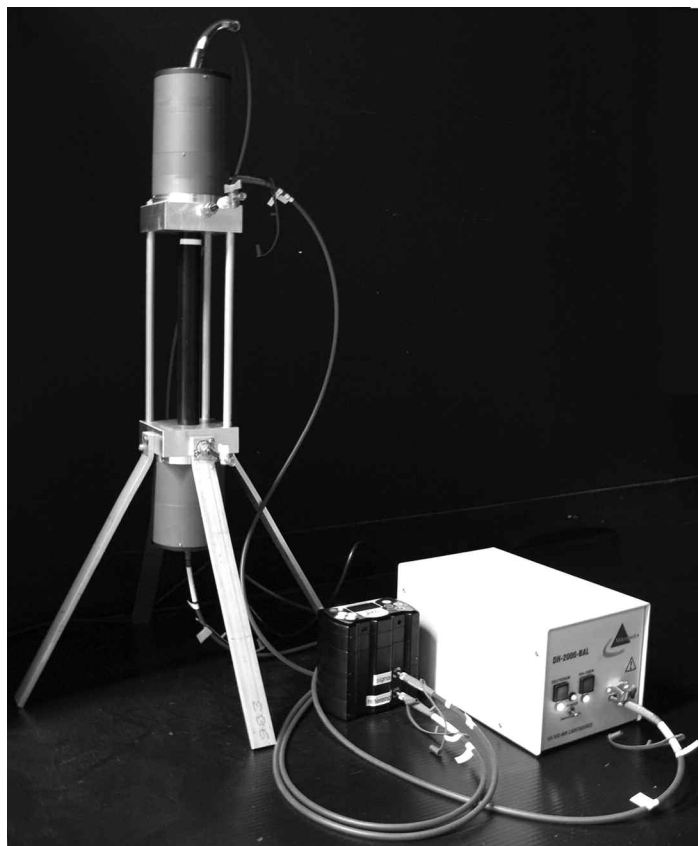
Fig. 1. The transmissometer system composed of a custom-built transmissometer, a fiber-coupled spectroscopic system, and a spectrally balanced light source (left to right).

trally balanced output between 200 and 1000 nm. The Jaz system collected the light simultaneously from both spectrometers: a signal channel and a reference channel used to monitor the output power and to correct the signal reading accordingly. Each of the spectrometers used a 2048-element linear silicon CCD array, configured with a 50-μm slit, and a grating (groove density = 600 mm⁻¹; blaze wavelength = 400 nm; grating #2, Ocean Optics) resulting in an effective spectral resolution of 2.06 nm (FWHM). A band-pass order-sorting filter (OFLV-QE, Ocean Optics) filtered higher orders of diffraction from the grating between 200 and 950 nm. Therefore, light collected by the CCD included only light from first-order diffraction, whereas, higher orders of diffraction that fall on different regions of the CCD (regions that correspond to other spectral ranges) were eliminated.

Transmissometer—The transmissometer's optical design followed the traditional collimated-beam design (Voss and Austin 1993) with a 25-cm path length (Fig. 2). To measure effects from both absorption and scattering, spatial filtering (1.3-mm aperture; Fig. 2i) ensured that light from a small acceptance angle is detected as described below. The transmissometer consisted of two optical assemblies, light emission and detection, with a flow tube, containing the water sample in between.
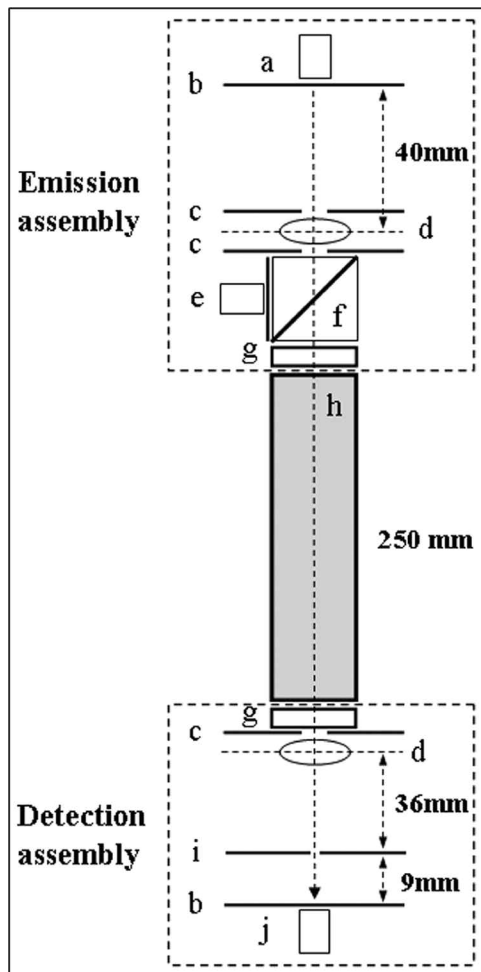
Fig. 2. The transmissometer optical setup. (a) Emitting optical fiber; (b) fiber holder; (c) 6 mm aperture; (d) 40 mm singlet lens; (e) reference optical fiber + diffusing Teflon film; (f) beamsplitter; (g) fused silica window; (h) flow tube; (i) 1.3 mm aperture; and (j) signal optical fiber + cosine corrector.

The various optical components used in each optical assembly were positioned in a rigid cage system, which made the transmissometer a robust instrument that could be deployed in the field near remote bodies of water. The cage system included 6 mm diameter rods (ER8, Thorlabs), SM1 fiber adaptors (Fig. 2b; SM1SMA, Thorlabs), threaded plates (CP02, Thorlabs) to hold the lenses (Fig. 2d; F = 40 mm; LA4306, Thorlabs), blank cage plates that were modified into apertures (Fig. 2c,i; plate thickness 1 mm; CP01, Thorlabs), a 4-way mounting cube (C6W, Thorlabs) that held a quartz beam splitter plate (Fig. 2f; Ealing 35-6121; ND = 0.5), a cosine corrector (CC-3-UV, Ocean Optics), and a 0.1-mm-thick Teflon film which served as diffuser, and fused silica windows (Fig. 2g; WG40530, Thorlabs).

Light emitted by the light source was guided by a 2 m optical fiber (core diameter 600 μm; numerical aperture 0.22 ± 0.02; acceptance angle 12.4°; 86%–95% transmission across 300–750 nm; QP600-2-UV-VIS; Ocean Optics) to the transmis-

someter. In the light emission assembly, light was collimated (beam width: 6 mm) and split into two beams using a beam splitter. One beam was transmitted through the water sample to the detection assembly, where it was channeled to one of the spectrometers by an optical fiber (signal channel). The other beam exited the transmissometer from the emission assembly and was guided to the second spectrometer by a second optical fiber (reference channel). A reference channel was necessary to monitor the optical source power and to correct the signal reading. The transmissometer had two openings fitted with valves, through which water samples were injected. For ease of handling, the transmissometer was positioned with the flow tube vertically aligned on four legs during measurements (Fig. 1).

Acceptance angle characterization—For a transmissometer to perform well, the acceptance angle of the collimated beam must be small, i.e., <1° (Voss and Austin 1993). The acceptance angle in air was measured by mounting the detection assembly on a rotation stage with the axis of rotation through the center of the focusing optics. Two optical sources were used: a monochromatic collimated beam (wavelength 633 nm, Helium-Neon laser, beam diameter 2.2 mm) and the beam from the emission assembly. The change in rotation angle of the detector assembly was measured by using a separate light source (collimated laser diode) directed at a mirror mounted on the side of the assembly and by monitoring the subsequent diode beam deflection 6 m away from the assembly. Light reaching the signal optical fiber was recorded for a wide range of assembly angles. The acceptance angle in air was determined from the half-width half-maximum of transmitted intensity as a function of assembly angle. To calculate the acceptance angle in water, the acceptance angle in air was divided by the water's refractive index at each wavelength (Austin and Halikas 1976; Quan and Fry 1995). The acceptance angle in water was determined to be 0.57° using the HeNe light source (Fig. 3). Note that the random uncertainty in the measurement is very small, but we estimate the systematic uncertainty in setting the assembly to zero deviation (incident beam normal to assembly and maximum transmission) was ~0.1°. To verify broadband performance, the output beam from the emission assembly was used in measuring the acceptance angle in air. Based on the latter, the acceptance angle in water was calculated to range 0.55 to 0.59° across the 300–750–nm spectral range, representing a systematic spectral difference of 7.6% (Fig. 3). This difference may be accounted for by the wavelength dependence of the refractive index of water (2.25%), wavelength dependence of the refractive index of the fused silica lens (2.3%), and various alignment imperfections. The small difference at 633 nm between the results with a monochromatic light source and that of the emission assembly (0.02°) arose due to imperfect collimation of the broadband light. For comparison, the value of the acceptance angle of the widely used spectral transmissometer ac-9 (WET Labs) was calculated by the manufacturer as 0.93° with a spec-
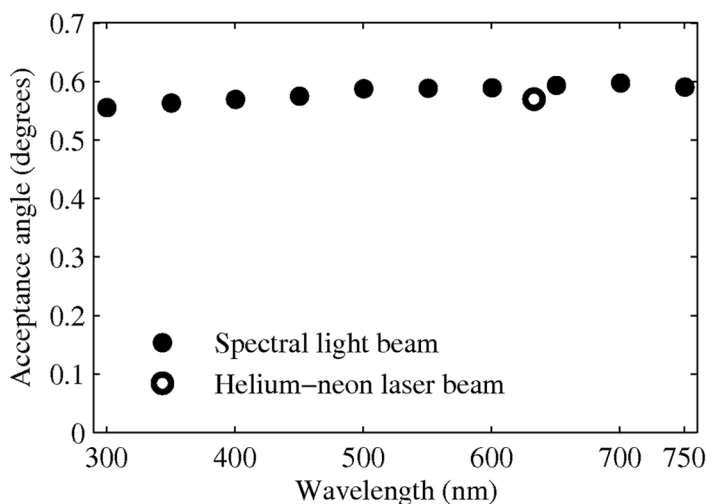
Fig. 3. The transmissometer acceptance angle in water as a function of wavelength (300–750 nm; 50-nm interval) measured with a spectral light beam and a 633-nm Helium-neon (HeNe) laser beam.

tral variability slightly higher (8%) for the 412–715 nm range (www.wetlabs.com/technicalnotes/technoteindex.htm).

Transmission measuring procedure—A measuring session included (i) disassembly of the transmissometer, thorough cleaning and reassembly of the instrument; and (ii) pure water calibration followed by measurement of the transmission of natural water.

Cleaning and reassembly of the transmissometer—The window at each end of the flow tube was cleaned using lens paper moistened with 99% ethanol. To clean the flow tube (Acrylonitrile-Butadiene-Styrene, ABS), a cotton-tipped applicator soaked with ethanol was slid through the flow tube, and then the flow tube was rinsed thoroughly with pure water and left to dry. Upon completion of the cleaning procedure, the transmissometer was reassembled and left untouched (neither disassembled nor moved) until the end of the measurement session. Thus we could reference the attenuation of natural water against the attenuation of pure water.

Pure water calibration and transmission measurement of natural water—Following the cleaning procedure, the light source and spectrometer were allowed to warm up for at least 40 minutes and pure water calibration was performed. As a pure water standard, we used water that was purified and filtered using a Milli-Q water purification system (Milli-Q Synthesis-10, Millipore) combining UV photooxidation and ultrafiltration, and resulting in pure water with nominal resistance of 18.2 MΩ cm. Pure water was left to sit for a few hours before performing a calibration in a 1 L acid washed High Density Polyethylene (HDPE) bottle (Nalgene). This allowed pure water to equilibrate with the ambient temperature, and for bubbles to come out or dissolve.

To measure the transmission of light through water, four different readings were acquired and saved: (i) signal light

reading—the light transmitted through the water sample; (ii) reference light reading—the light reading of the reference channel; (iii) signal dark reading—the dark reading of the signal channel and; (vi) reference dark reading— the dark reading of the reference channel. Signal and reference readings were acquired simultaneously. Dark readings were acquired when a mechanical shutter, built in the light source, was closed. The settings for both the signal and reference channels were identical: integration time was set to 6 s, the number of averaged spectra was 3, and the boxcar value (smoothing index) was 3. These settings provided sufficient signal-to-noise ratio, which resulted in low variation between separate pure water calibration trails.

For both pure water calibration and natural water measurement, water was gravity fed into the bottom valve of the transmissometer through opaque silicon tubing (inner diameter 3 mm). Initially, the flow tube (volume: 28 mL) was filled three times and purged completely. Therefore, an independent realization was achieved and successive water samples were treated as independent. Thereafter, water was gravity fed continuously, and the transmission readings were recorded. A flow rate of approximately 0.1 L/min was chosen to prevent particulate matter, suspended in the water sample, from sinking and collecting on the bottom window, while not inducing the formation of air bubbles. Note that the presence of air bubbles or an air interface between the windows and the water sample could be easily detected since the signal reading dropped off dramatically. However, we do not exclude the possibility that very small bubbles could have affixed to the top window without being detected. The temperature and the salinity of the natural water samples were recorded.

The purpose of the water calibration is to determine the offset values of attenuation that result in a zero reading with optically clean water in the sample volume of the flow tube. To confirm that the offset was precise, three water calibration trails were performed. Typically, a standard deviation <0.01 m^{-1}, ranging 0.0005–0.03 m^{-1} across the spectrum with no apparent spectral dependence, for the three water calibration trails was achieved. The average attenuation across the three water calibration trails was used as the water offset in the calculation of natural water attenuation. The transmission measurement of natural water samples commenced immediately following the pure water calibration and employed the same measurement procedure. The temperature of water (both pure and natural water samples) was measured using an electronic handheld thermometer (±0.1°C) and the salinity of water was measured using a mechanical hand-held refractometer (±1‰).

Data processing—Processing, including correction of the attenuation values for salinity and temperature, was performed following the general procedure described for the ac family transmissometer, WET Labs (Van Zee 2008). Specifically, measurements were made with the light source on ("sigLight"; "refLight") and shuttered off ("sigDark" and "ref-

Dark") for the signal and reference channels, respectively. Dark values were subtracted from light values (Eqs. 1 and 2). C stands for the measured value in digital counts for each pixel of the spectrometer's CCD (2–4 pixels per 1-nm wavelength). For readability, the wavelength dependence of all variables was omitted; however, this wavelength dependence is implicit in all variables described below.

$$C_{sig} = C_{sigLight} - C_{sigDark} \tag{1}$$

$$C_{ref} = C_{refLight} - C_{refDark} \tag{2}$$

The pure water offset, c_{off} [m^{-1}], was calculated as (Van Zee 2008):

$$c_{off} = -\frac{\ln\left(C_{wsig} / C_{wref}\right)}{x} \tag{3}$$

where C_{wsig} and C_{wref} represent the amount of light that reached the signal and reference detectors during the pure water calibration in raw digital counts, respectively. x represents the sample volume path length in meters, in our case 0.25 m. Since the number of CCD pixels corresponding to 1 nm wavelength varies with the light wavelength and spectrometer channel, count values of each channel were linearly interpolated to every 1 nm before calculation. To compute the attenuation of natural water, c [m^{-1}], and to apply the pure water offset, c_{off} [m^{-1}], the following algorithm was used (Van Zee 2008):

$$c = -\frac{\ln\left(C_{sig} / C_{ref}\right)}{x} - c_{off} \tag{4}$$

where C_{sig} and C_{ref} represent the amount of light that reached the signal and reference detectors during the measurement of natural water in raw digital counts, respectively.

To account for differences in the temperature and salinity between pure water (during calibration) and natural water (during measurement), a correction procedure was applied. Temperature and salinity effects on pure water scattering were removed from the measured attenuation, c, using the algorithm:

$$c_{t,s\ sca} = c - (bw_{t,s} - bw_{tr,sr}) \tag{5}$$

where $c_{t,s\ sca}$ [m^{-1}] is the attenuation corrected for the temperature and salinity dependences of scattering. $bw_{t,s}$ [m^{-1}] represents the scattering coefficient of water at temperature (t) and salinity (s) (of natural water during measurement), and $bw_{tr,sr}$ [m^{-1}] represents the scattering coefficient of water at the reference temperature (tr) and reference salinity (sr) (of pure water during calibration). The scattering coefficient was calculated following the theoretical model developed by Zhang et al. (2009) at a 1-nm interval. This model takes into account the effects of concentration and density fluctuation on the scat-

tering by pure water (depolarization ratio was set to 0.039). This model was suggested to be applicable for wavelengths between 200 and 1100 nm (Huibers 1997), temperature of 0 to 30°C, and salinity of 0–40‰ (Zhang et al. 2009).

Temperature and salinity effects on pure water absorption were removed using the algorithm (Van Zee 2008):

$$c_{t,s\ abs} = c - \left[\Psi_t \cdot (t - tr) + \Psi_s \cdot (s - sr)\right] \tag{6}$$

where $c_{t,s\ abs}$ [m^{-1}] is the attenuation corrected for the temperature and salinity dependences of absorption and Ψ_t [m^{-1} °C] and Ψ_s [m^{-1} ‰] are the temperature and salinity correction factors, respectively (see Sullivan et al. [2006] for discussion on the practical similarity between ‰ and Practical Salinity Scale). To conform to the high spectral resolution of our transmissometer (2.06 nm), temperature correction factors, Ψ_t for wavelengths between 550 and 750 nm were adopted from Langford et al. (2001) (obtained with a 2-nm band pass), whereas correction factors for wavelengths between 400 and 550 nm were taken from Pegau and Zaneveld (1993) and Pegau et al. (1997) (obtained with a 10-nm band pass). These correction factors are valid for temperatures between 15°C and 30°C and are given at varying spectral intervals. Therefore, correction factors were linearly interpolated at a 1-nm interval. To take advantage of the entire spectral range of the transmissometer (300–750 nm), temperature correction factors between 300 and 400 nm were set to zero. This is likely to be a good approximation because the temperature correction factor at the shortest available wavelength (400 nm) is smaller than 10^{-4} m^{-1}°C, and the temperature dependence increases with wavelength in this spectral region. Salinity correction factors, Ψ_s [m^{-1} ‰] were adopted from Sullivan et al. (2006). Although determined using a relatively broad spectral band pass (14–18 nm), to date this set of correction factors is the most complete and spectrally broad available.

Temperature and salinity also affect the water's refraction index, and hence the transmission of light through the fused-silica window-water interface. Attenuation measurements were corrected for these changes in transmission through the water-window interface, as they induce a small yet easily corrected bias (*see* "Comments and recommendations"). The refractive index of water was calculated using the empirical equation developed by Quan and Fry (1995), which reproduces the indices measured by Austin and Halikas (1976). The water's refractive index and the transmission of light through the window-water interface were calculated once for the temperature and salinity conditions during the calibration (T_r) and second for the conditions during the measurement of natural water (T). Transmission was calculated as

$$T = \left[1 - \left(\frac{n_{fs} - n_w}{n_{fs} + n_w}\right)^2\right]^2 \tag{7}$$

where n_{fs} and n_w are the refractive indices of fused silica and water, respectively (Hecht 2002). To correct the measured attenuation for changes in transmission, the following algorithm was used:

$$c_T = c + \frac{1}{x} \cdot \ln(T / T_r) \qquad (8)$$

where c_T [m^{-1}] is the attenuation corrected for the temperature and salinity dependence of transmission.

Assessment

Transmissometer precision and dynamic range—The raw precision of the system was examined both in air and water. Precision was determined by calculating the standard deviation of twenty-five transmission readings, taken successively during 1 h. In air, precision averaged 0.011 m^{-1} and varied between 0.005 and 0.024 m^{-1} across the 300–750–nm spectral range (Fig. 4A; integration time: 6 s; number of averaged spectra: 3). The lowest precision was attained in the region between 300 and 450 nm, which corresponds to the spectral range where the light source output was lowest. Using the same spectrometer settings, precision in water averaged 0.012 m^{-1} and varied between 0.007 and 0.023 m^{-1} across the spectrum (Fig. 4A). Here again, the lowest precision was obtained between 300 and 450 nm. Additionally, the precision in water was also examined throughout a longer period (3 h, $n = 10$), with readings taken every 20 min and averaged 0.013 m^{-1} (ranging 0.006–0.029 m^{-1} across the spectrum).

To validate the spectral precision of the transmissometer, we measured the attenuation of a Holmium wavelength calibration standard. Holmium perchlorate (15% wt/vol in perchloric acid; H8015 Lot# 019K8713; Sigma-Aldrich) was diluted 100-fold with pure water and stored in acid-washed amber glass bottles with Teflon-lined caps at room temperature. The attenuation of the Holmium perchlorate solution was measured in triplicate within 1 hour of preparation. The characteristic attenuation peaks of Holmium perchlorate ranging from 333 to 640 nm could be clearly detected (Fig. 4B). Spectral locations of attenuation peaks were shifted to longer wavelengths by 0.67 ± 0.26 nm from those provided by the manufacturer. Thus, this assessment stage validates the applicability of the transmissometer in detecting attenuation peaks in high precision throughout the spectrum examined.

The transmissometer has a possible maximum dynamic range of 48 dB (16-bit). Due to detector noise, for the integration time used (6 s), the observed dynamic range was 35 dB, which permitted a measurement across 3.5 orders of magnitude. At extreme attenuation levels, however, there is a greater probability of multiple scattering, which can cause an underestimation of the true attenuation. Consequently, the transmissometer's precision and dynamic range characteristics ensure accurate and reliable readings of the attenuation for water bodies spanning from the clear open ocean (Barnard et
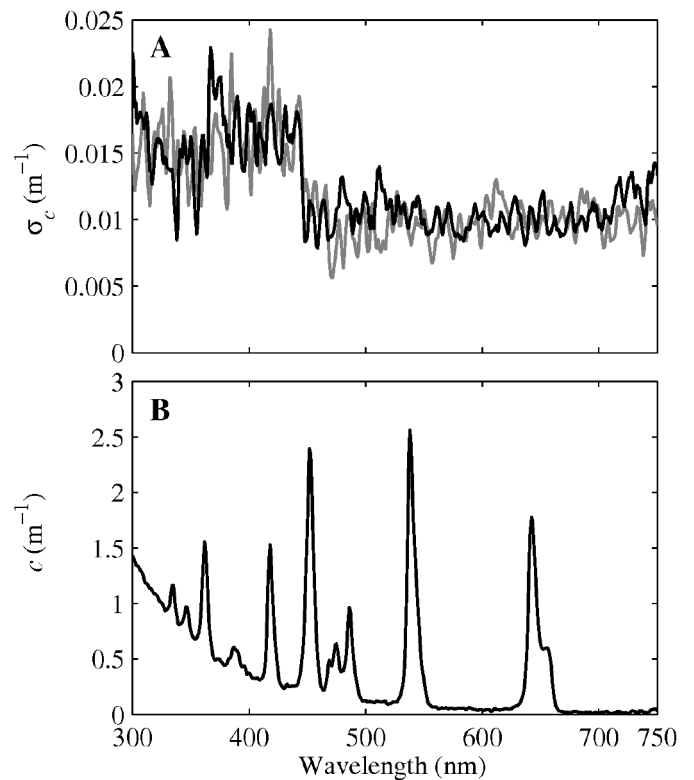
Fig. 4. The transmissometer's precision in measuring beam attenuation for air (gray) and pure water (black) (A). Precision was determined by calculating the standard deviation (σ_c) of twenty-five transmission readings taken successively during 1 h. The discontinuity at 430 nm is due to the output of the two lamps of the light source (Tungsten-Halogen and Deuterium) merging. The attenuation of Holmium perchlorate (B). The characteristic attenuation peaks of Holmium perchlorate can be clearly detected.

al. 1998) to the extremely turbid water of rivers and estuaries (Campbell and Spinrad 1987; Wells and Kim 1991).

Transmissometer performance in the visible spectral range—To assess the performance of the transmissometer system in the visible range, we compared the attenuation measured by our transmissometer against that measured using the commercially available ac-s transmissometer (WET labs). The spectral range compared was limited by the ac-s to 400–736 nm. Both transmissometers are equipped with a 25 cm flow tube but differ in acceptance angle (0.57° and 0.93° for our transmissometer and the ac-s, respectively). Additionally, the ac-s exhibits a variable spectral band pass of 14–18 nm whereas the effective spectral resolution of our transmissometer is 2.06 nm (FWHM). Thus, to compare the two instruments, spectral attenuation curves measured using our transmissometer were smoothed with a moving average of ±8 nm. River and pond water samples and a sample of seawater enriched with phytoplankton (chlorophyll ~15 mg m^{-3}) were analyzed in triplicate using both instruments. River water was collected from the Stillwater River next to the University of Maine's campus, Orono, Maine, USA; pond water was collected from a rainwa-

ter runoff pond next to the University of Maine's campus; and seawater was collected from the Darling Marine Center's Dock, University of Maine, Walpole, Maine, USA. All samples were measured for the attenuation due to particulate and dissolved matter (c_{pg}). To measure the attenuation due to dissolved matter alone, water samples were filtered using a 0.22-μm filter (500-mL bottle-top polyethersulfone filter; Corning). Water samples were gravity fed into the bottom valve of the ac-s flow tube and exited through the upper valve. Processing of the ac-s data were previously described elsewhere (Twardowski et al. 1999). Pure water calibration, transmission measurement of natural water, and data processing for our transmissometer system were performed following the procedures described

above. Both instruments were calibrated using optically pure water (Barnstead NANOpure).

For the river and pond water samples, c_{pg} measured by the two instruments was significantly similar (assessed by overlap of data within three standard deviations; i.e., the 95% confidence interval) with standard deviation averaged across the spectrum for the transmissometer: 0.006 and 0.11 m^{-1} and ac-s: 0.052 and 0.063 m^{-1}, respectively (Fig. 5C,E). However, c_{pg} of the seawater enriched with phytoplankton differed significantly between instruments with standard deviation averaged across the spectrum of 0.004 m^{-1} for the transmissometer and 0.022 m^{-1} for the ac-s (Fig. 5A). c_g measured by the two instruments did not differ significantly with standard deviation
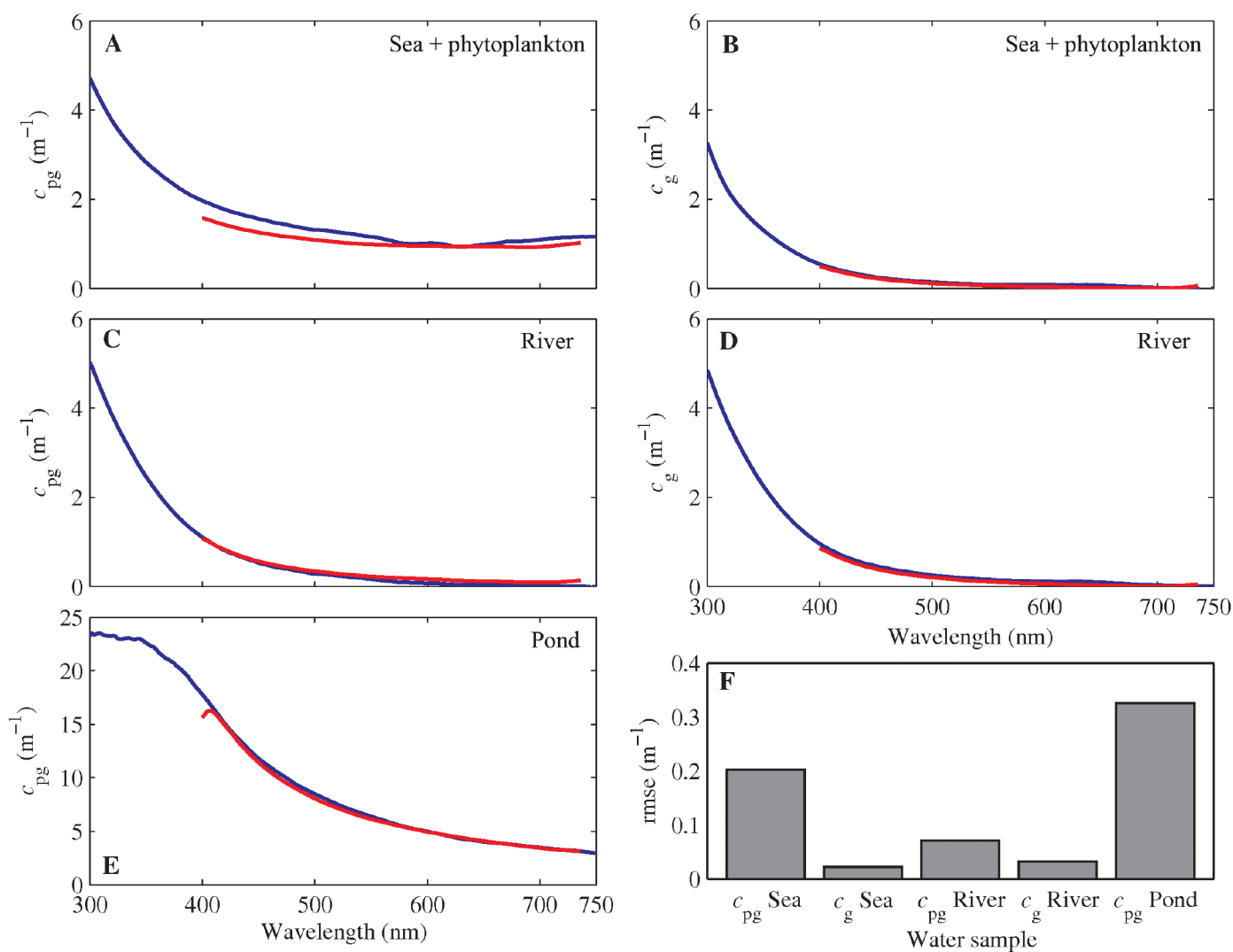
Fig. 5. Comparison between the spectral attenuation measured by our transmissometer (blue) and the WET labs ac-s transmissometer (red). The attenuation due to particulate and dissolved matter (c_{pg}) was measured for seawater enriched with phytoplankton (A), and river (C) and pond (E) water samples. The attenuation due to dissolved matter alone (c_g) was measured for seawater enriched with phytoplankton (B) and river (D) samples. c_{pg} deviated slightly between the two instruments, with the highest deviation observed for the seawater sample. On the other hand, c_g measured by the two instruments correlates well. The root mean squares error in attenuation measured by the two instruments is depicted in (F). Panel E shows that whereas the ac-s fails to adequately describe attenuations above 15 m^{-1}, our transmissometer performs well at attenuations up to ~20 m^{-1}.

averaged across the spectrum for the transmissometer: 0.004 and 0.027 m^{-1} and ac-s: 0.003 and 0.002 m^{-1}, for the seawater enriched with plankton and river water, respectively (Fig. 5B,D). The root mean squares error (rmse) of attenuation measured by the two instruments was 0.2 and 0.07 m^{-1} for c_{pg}, but only 0.02 and 0.03 m^{-1} for c_g of the seawater and plankton, and river water, respectively (Fig. 5F). The relatively large deviation in c_{pg} between instruments is in agreement with the difference in the instruments' acceptance angles. Typically, attenuation values vary with instrument acceptance angle, where smaller acceptance angles provide higher beam attenuation values (Boss et al. 2009). This difference is due to variations in scattered light collected with different acceptance angles and is nicely illustrated by the c_{pg} of seawater enriched with phytoplankton (Fig. 5A). In this case, phytoplankton particles intensely scatter light that is more efficiently collected by the larger acceptance angle of the ac-s. The attenuation difference between instruments decreased with the removal of scattering particles from the samples (c_g; Fig. 5B,D). Moreover, Fig. 5E shows that while the ac-s fails to adequately describe attenuations above 15 m^{-1}, our transmissometer performs well at attenuations of up to approximately 20 m^{-1}.

This stage of assessment was performed by EB's lab technician, who did not take part in developing and characterizing the transmissometer. This lab technician successfully assembled the transmissometer and performed all calibration and measurement procedures following a draft user manual, illustrating the ease of setting up and operating the transmissometer.

Transmissometer performance in the ultraviolet spectral range— To assess the performance of the transmissometer system in the UV range, the attenuation due to dissolved matter (c_g) was compared against the absorption of dissolved matter (a_g) measured with a bench-top spectrometer. c_g is the sum of the absorption (a_g) and scattering (b_g) due to dissolved matter. Because the scattering of dissolved matter is negligible (Stramski and Wozniak 2005), c_g and a_g are expected to be comparable. Measurements of absorption were performed using a UV-visible bench-top spectrometer (Cary 300 Bio; Varian) in a 1 cm quartz cuvette. Ten replicate scans of absorption were made from 300 to 750 nm at 1-nm intervals and a spectral band width of 2 nm. For this validation stage, surface water was collected from Lake Ontario, Kingston, Canada. The original sample and a 2-fold diluted sample were analyzed. To avoid any temperature differences between samples and reference (optically pure water), samples were kept in a dark compartment and left to equilibrate with room temperature for a few hours. Prior to measurement, samples were filtered through a 0.22-μm filter (*see* specifications above). The spectral absorption due to dissolved matter, $a_g(\lambda)$ [m^{-1}], was calculated by multiplying the measured absorption by ln(10) and dividing by the path length (0.01 m). Slightly negative absorption values were occasionally observed when absorption was extremely weak, which occurred in the near-infrared spectral region (700–750 nm). Accordingly, all spectra were corrected by subtracting the low-

est value in the near-infrared region from $a_g(\lambda)$ at all wavelengths (Babin and Stramski 2002, 2004).

Attenuation (c_g) and absorption (a_g) due to dissolved matter did not differ significantly, with standard deviation averaged across the spectrum of c_g: 0.01 and 0.01 m^{-1} and a_g: 0.08 and 0.22 m^{-1}, for stock and diluted samples, respectively (Fig. 6). The rmse between c_g and a_g was 0.16 and 0.07 m^{-1} for the stock and the diluted samples, respectively. c_g at 300–360 nm was slightly larger than a_g, likely the contribution of scattering by particles smaller than 0.22 μm that passed through the filter (Arnott and Marston 1988; Morel 1991; Stramski and Kiefer 1991). Such scattered light will be captured by the bench-top spectrophotometer more efficiently than by the transmissometer with its narrow acceptance angle, resulting in a decrease in a_g but not in c_g. Moreover, on the basis of theoretical considerations, scattering by such particles is larger at shorter wavelengths (Bohren and Huffman 1983), thus supporting our observation.

Transmissometer field test—Water samples were collected on 21 July 2008 at Mitande, a near shore site on the southern shore of Thumbi West Island, Lake Malawi, Africa (14°01'36.51" S 34°49'26.61" E). This site had a bottom depth of 11 m and was composed of mixed rocks and sandy patches. Samples were collected along a vertical depth profile (5 points between 1 and 10 m of depth). Three samples of natural water were collected at each point along the measurement profile and their measured attenuation values were averaged. Analysis of natural water samples commenced 1 h following collection. During this time period, water samples were kept in a cool and dark compartment. Water samples were gently
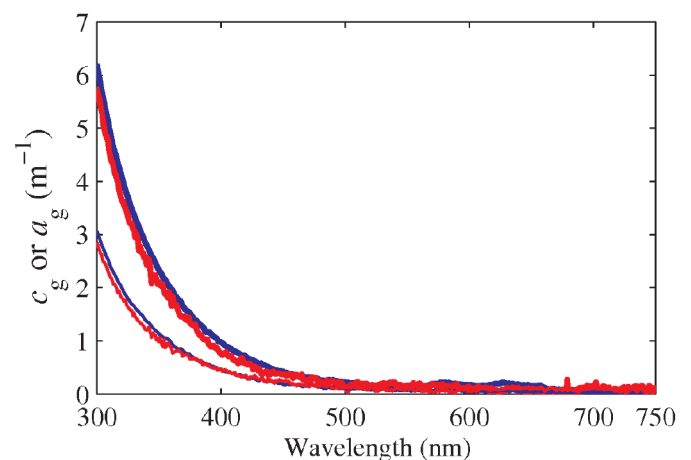
Fig. 6. Comparison between the spectral attenuation due to dissolved matter (c_g; blue) measured by our transmissometer and the spectral absorption due to dissolved matter (a_g; red) measured with a bench-top spectrometer of stock (thick lines) and 2-fold diluted (thin lines) samples. c_g and a_g behave similarly across the spectrum with very good agreement in their absolute values, although deviating slightly in the UV spectral range. The variation as a function of wavelength in a_g is a result of the short path length of the cuvette (1 cm), and consequently, the low sensitivity of the measurement.

shaken before measurements. However, we do not exclude the possibility of particles settling. Spectral attenuation due to dissolved and particulate matter, $c_{pg}(\lambda)$, attained a maximum value of 1.1 m^{-1} at the shortest wavelength examined (300 nm) and decreased with wavelength (Fig. 7) following a power-law function of the form: $c_{pg}(\lambda) = c_{pg}(\lambda_r)(\lambda/\lambda_r)^{-\gamma}$, where λ_r is a reference wavelength (660 nm) and γ is the power-law exponent describing the relative steepness of the c_{pg} spectrum (Boss et al. 2001). Least-squares fitting of the power-law function to the c_{pg} data resulted in rmse less than 0.035 m^{-1} (across all depths) and a spectral slope parameter, γ, ranging from 1.51 to 2.237. To the best of our knowledge, the attenuation due to particulate and dissolved matter has never been reported for Lake Malawi (neither the attenuation of each of the constituents alone). However, the γ values obtained and the magnitude of attenuation at 660 nm ($c_{pg}[660]$; ranging 0.158–0.283 m^{-1}) are in general agreement with the range of previously reported slope and attenuation values for other locations, γ: 0.5–2.3, c_{pg}: 0.1–1.5 m^{-1} (Boss et al. 2001; Chang and Dickey 2001; Souza et al. 2001).

Discussion

The portable hyperspectral beam transmissometer developed in our lab is capable of measuring across a broad spectral range (300–750 nm) at 2 nm spectral resolution. The transmissometer exhibits a small acceptance angle (0.55 to 0.59° across the spectrum), a well collimated spectral light beam, and precision of ±0.012 m^{-1} (averaged across the spectrum). The transmissometer was shown to detect absorption peaks with a high spectral precision (0.67 ± 0.26 nm). The attenuation measured using our transmissometer was compared against a commercially available transmissometer and a bench-top spectrometer, confirming its accuracy between 300 and 750 nm for both attenuation due to particulate and dis-

Fig. 7. Spectral attenuation due to dissolved and particulate matter, c_{pg}, at 5 depths at Thumbi West Island, Lake Malawi, Africa.

solved matter, and attenuation due to dissolved matter alone. Throughout the assessment, lake, river, pond, and seawater samples were successfully analyzed, illustrating the wide-ranging applicability of the transmissometer. Additionally, the performance of the transmissometer was demonstrated under field conditions, where the transmission of water samples collected from Lake Malawi, Africa, was measured on site.

The transmissometer system is fully portable. The Jaz spectroscopic system (weight: 1.1 kg) includes a powerful microprocessor and onboard display, allowing the operator to change the spectrometers' settings, acquiring and saving spectrometer files without the need to interface a PC. The Jaz system includes three slots for SD memory cards, allowing the system to store several gigabytes of data (1 GB = ~28,000 spectrometer files). Additionally, it is equipped with a rechargeable Lithium-Ion battery module that can power the system for up to 8 h. The spectrally balanced light source (weight: 3.8 kg) can be powered by a car battery for several hours (and actually was during the field tests in Lake Malawi). All these features make the transmissometer system fully self-sufficient and highly portable, providing measuring capabilities for the most remote locations on land or at sea. The fabrication of the transmissometer was relatively simple and inexpensive. The total cost of parts and labor was under 1000 USD. In addition, the light source (DH-2000-BAL, Ocean Optics) and the fiber-coupled spectroscopic system (Jaz, Ocean Optics) cost approximately 4500 and 3500 USD, respectively.

The transmissometer system provides a substantial advance, in comparison with commercially available instruments that are capable of measuring absorption in the UV spectral range. The absorption of dissolved matter across the UV-visible range can be measured using a bench-top spectrometer. However, due to their high weight and large dimensions, bench-top spectrometers are typically restricted to the laboratory environment. In contrast, our hyperspectral transmissometer system is portable and power self-sufficient, and thus has functional advantages over any bench-top spectrometer. The spectral range of the ISUS (Satlantic) is limited to 200–400 nm. Although it might be used as a spectrophotometer to measure the absorption of dissolved matter, the ISUS is marketed as a nitrate sensor. Moreover, because the ISUS is equipped with a 1-cm path length, its sensitivity is lower than that of our transmissometer (25-cm path length). Finally, unlike the ISUS, our transmissometer system is capable of measuring the absorption of dissolved matter, the attenuation due to dissolved matter, or the attenuation of both dissolved and particulate matter across the UV-visible spectrum. Our transmissometer system demonstrates significant advantages over bench-top spectrometers and the ISUS nitrate sensor.

In summary, the transmissometer developed in our laboratory met our mission objectives. The transmissometer is fully portable and self-sufficient, relatively low cost, easy to assemble and operate, and measures the attenuation at the accuracy and precision required for many oceanographic and aquatic
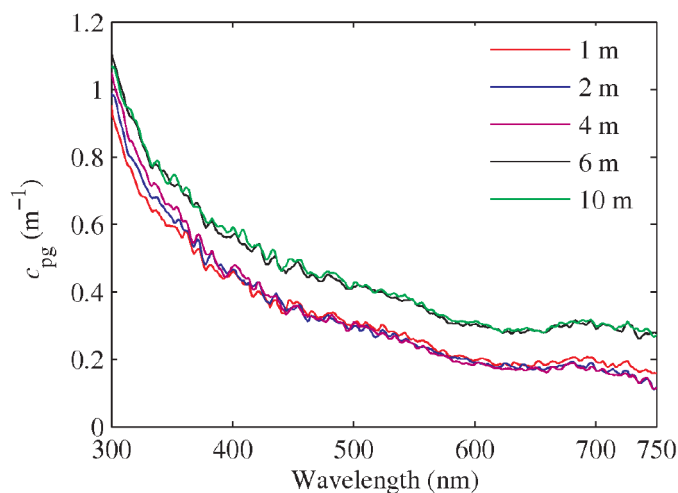
biology studies across the UV-visible spectrum. The extended spectral range and high spectral resolution of the transmissometer make it an excellent tool for studying the spectral characteristics of the attenuation due to dissolved and particulate matter and the absorption of dissolved matter in aquatic media, and their spatial distribution in the environment. For those researchers studying visual biology, our transmissometer provides important information characterizing the optic conditions of aquatic ecosystems that impose constraints on visibility, essential to visual communication in aquatic organisms.

Comments and recommendations

Dissolved material and chlorophyll in natural water may fluoresce (Gordon 1979; Carder et al. 1989). Light emitted at a given wavelength may excite these fluorophores to emit at longer wavelengths. Hence, the small percentage of fluorescence that is emitted within the acceptance angle is included in the measurement. Consequently, the attenuation at longer wavelengths could be a slight underestimation of the real attenuation at a fluorescing waveband. The potential contribution of fluorescence to the measured attenuation can be easily constrained. For CDOM, approximately 1% of photons absorbed might be re-emitted nearly isotropically by fluorescence. Given the acceptance angle of the transmissometer (0.57° or 0.00124 steradian), only 0.0001% of photons absorbed might be re-emitted and collected by the transmissometer's acceptance angle. Apart from fluorescence, another process that may contribute to the measurement error is Raman (inelastic) scattering. However, the cross-section for Raman scattering is very small, and because it occurs in both pure and natural waters, calibration removes its contribution.

Salinity and temperature might affect the acceptance angle of the transmissometer through their effect on the refractive index of water, n_w. To assess the potential magnitude of this effect, n_w was calculated for salinities 0–40‰, temperatures 0 to 30°C, and wavelengths 300–750 nm following Quan and Fry (1995). n_w increases with salinity but decreases with temperature. The effect of both salinity and temperature on n_w is reciprocal to wavelength. That is, the largest difference in the refractive index of water due to salinity and temperature variation is attained at a wavelength of 300 nm and with temperature and salinity varying from 30°C to 0°C and 0‰ to 40‰, respectively. In this most extreme case, n_w would vary between 1.3584 and 1.3693, corresponding to a refractive index difference of 0.796%. Following Snell's law, such a difference in n_w would result in a comparable difference in the angle of the refraction (Hecht 2002), and thus, in the acceptance angle of the transmissometer, a change of 0.00453°. This change in acceptance angle would increase the pure water offset by 0.0027 m^{-1} (calculated using Eqs. 7 and 8).

References

Arnott, W. P., and P. L. Marston. 1988. Optical glory of small freely rising gas-bubbles in water - observed and computed cross-polarized backscattering patterns. J. Opt. Soc. Am. A Image Sci. Vis. 5: 496-506.

Austin, R. W., and G. Halikas. 1976. The index of refraction of seawater. Scripps Institution of Oceanography. SIO Ref. 76-1.

Babin, M., and D. Stramski. 2002. Light absorption by aquatic particles in the near-infrared spectral region. Limnol. Oceanogr. 47: 911-915.

Babin, M., and D. Stramski. 2004. Variations in the mass-specific absorption coefficient of mineral particles suspended in water. Limnol. Oceanogr. 49: 756-767.

Baker, E. T., and J. W. Lavelle. 1984. The effect of particle-size on the light attenuation coefficient of natural suspensions. J. Geophys. Res. 89:8197-8203 [doi:10.1029/JC089iC05p08197].

Barnard, A. H., W. S. Pegau, and J. R. V. Zaneveld. 1998. Global relationships of the inherent optical properties of the oceans. J. Geophys. Res. 103:24955-24968 [doi:10.1029/98JC01851].

Barth, H., K. Grisard, K. Holtsch, R. Reuter, and U. Stute. 1997. Polychromatic transmissometer for in situ measurements of suspended particles and gelbstoff in water. Appl. Opt. 36:7919-7928 [doi:10.1364/AO.36.007919].

Bohren, C. F., and D. Huffman. 1983. Absorption and scattering of light by small particles. John Wiley.

Boss, E., W. S. Pegau, W. D. Gardner, J. R. V. Zaneveld, A. H. Barnard, M. S. Twardowski, G. C. Chang, and T. D. Dickey. 2001. Spectral particulate attenuation and particle size distribution in the bottom boundary layer of a continental shelf. J. Geophys. Res. 106:9509-9516 [doi:10.1029/2000JC900077].

———, W. H. Slade, M. Behrenfeld, and G. Dall'olmo. 2009. Acceptance angle effects on the beam attenuation in the ocean. Opt. Express 17:1535-1550 [doi:10.1364/OE.17.001535].

Campbell, D. E., and R. W. Spinrad. 1987. The relationship between light attenuation and particle characteristics in a turbid estuary. Estuar. Coast. Shelf Sci. 25:53-65 [doi:10.1016/0272-7714(87)90025-4].

Carder, K. L., R. G. Steward, G. R. Harvey, and P. B. Ortner. 1989. Marine humic and fulvic-acids—their effects on remote-sensing of ocean chlorophyll. Limnol. Oceanogr. 34:68-81 [doi:10.4319/lo.1989.34.1.0068].

Chang, G. C., and T. D. Dickey. 2001. Optical and physical variability on timescales from minutes to the seasonal cycle on the New England shelf: July 1996 to June 1997. J. Geophys. Res. 106:9435-9453 [doi:10.1029/2000JC900069].

Diehl, P., and H. Haardt. 1980. Measurement of the spectral attenuation to support biological-research in a plankton tube experiment. Oceanol. Acta 3:89-96.

Field, C. B., M. J. Behrenfeld, J. T. Randerson, and P. Falkowski. 1998. Primary production of the biosphere: Integrating terrestrial and oceanic components. Science 281:237-240 [doi:10.1126/science.281.5374.237].

Gordon, H. R. 1979. Diffuse reflectance of the ocean—theory

of its augmentation by chlorophyll-a fluorescence at 685-nm. Appl. Opt. 18:1161-1166 [doi:10.1364/AO.18.001161].

Hawryshyn, C. W., and R. Beauchamp. 1985. Ultraviolet photosensitivity in goldfish—an independent UV retinal mechanism. Vision Res. 25:11-20 [doi:10.1016/0042-6989(85)90075-6].

Hecht, E. 2002. Optics, 4th ed. Addison Wesley.

Huibers, P. D. T. 1997. Models for the wavelength dependence of the index of refraction of water. Appl. Opt. 36:3785-3787 [doi:10.1364/AO.36.003785].

Jerlov, N. G. 1976. Marine optics. Elsevier.

Johnson, K. S., and L. J. Coletti. 2002. In situ ultraviolet spectrophotometry for high resolution and long-term monitoring of nitrate, bromide and bisulfide in the ocean. Deep Sea Res. I 49:1291-1305 [doi:10.1016/S0967-0637(02)00020-1].

Langford, V. S., A. J. Mckinley, and T. I. Quickenden. 2001. Temperature dependence of the visible-near-infrared absorption spectrum of liquid water. Journal of Physical Chemistry A 105:8916-8921 [doi:10.1021/jp010093m].

Losey, G. S., T. W. Cronin, T. H. Goldsmith, D. Hyde, N. J. Marshall, and W. N. McFarland. 1999. The UV visual world of fishes: A review. J. Fish Biol. 54:921-943 [doi:10.1111/j.1095-8649.1999.tb00848.x].

Lundgren, B. 1975. Measurements in the Baltic with a spectral transmittance meter. University of Copenhagen Institute of Physics and Oceanography Report nr 30.

Lythgoe, J. N., and J. C. Partridge. 1991. The modeling of optimal visual pigments of dichromatic teleosts in green coastal waters. Vision Res. 31:361-371 [doi:10.1016/0042-6989(91)90089-N].

Marshall, J., T. W. Cronin, and S. Kleinlogel. 2007. Stomatopod eye structure and function: A review. Arthro. Struct. Delundgrenvelop. 36:420-448 [doi:10.1016/j.asd.2007.01.006].

Marshall, N. J., K. Jennings, W. N. McFarland, E. R. Loew, and G. S. Losey. 2003. Visual biology of Hawaiian coral reef fishes. III. Environmental light and an integrated approach to the ecology of reef fish vision. Copeia 467-480 [doi:10.1643/01-056].

Matlack, D. E. 1974. Deep ocean optical measurements (dom) report on north Atlantic, Caribbean, and Mediterranean cruises. Technical Report Naval Ordnance Lab 1-103.

———, and J. R. V. Zaneveld. 1993. Temperature-dependent absorption of water in the red and near-infrared portions of the spectrum. Limnol. Oceanogr. 38:188-192 [doi:10.4319/lo.1993.38.1.0188].

Morel, A. 1991. Light and marine photosynthesis - a spectral model with geochemical and climatological implications. Prog. Oceanogr. 26: 263-306.

Pegau, W. S., D. Gray, and J. R. V. Zaneveld. 1997. Absorption and attenuation of visible and near-infrared light in water: Dependence on temperature and salinity. Appl. Opt. 36:6035-6046 [doi:10.1364/AO.36.006035].

Petzold, T. J., and R.W. Austin (1968). An underwater transmissometer for ocean survey work. Visibility Laboratory.

Scripps Institution of Oceanography, University of California. San Diego. SIO Ref. 68-9.

Quan, X. H., and E. S. Fry. 1995. Empirical-equation for the index of refraction of seawater. Appl. Opt. 34:3477-3480 [doi:10.1364/AO.34.003477].

Sabbah, S., and N. Shashar. 2006. Polarization contrast of zooplankton: A model for polarization-based sighting distance. Vision Res. 46:444-456 [doi:10.1016/j.visres.2005.05.017].

Souza, A. J., T. D. Dickey, and G. C. Chang. 2001. Modeling water column structure and suspended particulate matter on the middle Atlantic continental shelf during the passages of hurricanes Edouard and Hortense. J. Mar. Res. 59:1021-1045 [doi:10.1357/00222400160497751].

Spinrad, R. W., and J. R. V. Zaneveld. 1982. An analysis of the optical-features of the near-bottom and bottom nepheloid layers in the area of the Scotian rise. J. Geophys. Res. 87:9553-9561 [doi:10.1029/JC087iC12p09553].

Stramski, D., and D. A. Kiefer. 1991. Light-scattering by microorganisms in the open ocean. Prog. Oceanogr. 28:343-383 [doi:10.1016/0079-6611(91)90032-H].

———, and S. B. Wozniak. 2005. On the role of colloidal particles in light scattering in the ocean. Limnol. Oceanogr. 50:1581-1591 [doi:10.4319/lo.2005.50.5.1581].

Sullivan, J. M., M. S. Twardowski, J. R. V. Zaneveld, C. M. Moore, A. H. Barnard, P. L. Donaghay, and B. Rhoades. 2006. Hyperspectral temperature and salt dependencies of absorption by water and heavy water in the 400-750 nm spectral range. Appl. Opt. 45:5294-5309 [doi:10.1364/AO.45.005294].

Twardowski, M. S., J. M. Sullivan, P. L. Donaghay, and J. R. V. Zaneveld. 1999. Microscale quantification of the absorption by dissolved and particulate material in coastal waters with an ac-9. J. Atmos. Ocean. Technol. 16:691-707 [doi:10.1175/1520-0426(1999)016<0691:MQOTAB>2.0.CO;2].

———, E. Boss, J. B. Macdonald, W. S. Pegau, A. H. Barnard, and J. R. V. Zaneveld. 2001. A model for estimating bulk refractive index from the optical backscattering ratio and the implications for understanding particle composition in case I and case II waters. J. Geophys. Res. 106:14129-14142 [doi:10.1029/2000JC000404].

Vahatalo, A. V., and R. G. Wetzel. 2004. Photochemical and microbial decomposition of chromophoric dissolved organic matter during long (months-years) exposures. Mar. Chem. 89:313-326 [doi:10.1016/j.marchem.2004.03.010].

Van De Hulst, H. C. 1957. Light scattering by small particles. Dover.

Van Zee, H. 2008. Ac meter protocol. WET Labs.

Volz, F. 1954. Die Optik und meteorologie der atmospharisehen triibung. Ber. Dtseh. Wetterd. 13:1-47.

Voss, K. J., and R. W. Austin. 1993. Beam-attenuation measurement error due to small-angle scattering acceptance. J. Atmos. Ocean. Technol. 10:113-121 [doi:10.1175/1520-0426(1993)010<0113:BAMEDT>2.0.CO;2].

Wells, J. T., and S. Y. Kim. 1991. The relationship between beam transmission and concentration of suspended particulate material in the Neuse River estuary, North Carolina. Estuaries 14:395-403 [doi:10.2307/1352264].

Zepp, R. G. 2003. Solar uvr and aquatic carbon, nitrogen, sulfur and metal cycles, p. 137-183. *In* E. W. Helbling and H. Zagarese [eds.], Comprehensive series in photochemical and photobiological sciences. European Society for Photobiology.

Zhang, X. D., L. B. Hu, and M. X. He. 2009. Scattering by pure seawater: Effect of salinity. Opt. Express 17:5698-5710 [doi:10.1364/OE.17.005698].